On the knee of Galactic cosmic rays in light of sub-TeV spectral hardenings*

Yi-Qing Guo(郭义庆)[1,2] Qiang Yuan(袁强)[1,3;1)]

[1] Key Laboratory of Dark Matter and Space Astronomy, Purple Mountain Observatory, Chinese Academy of Sciences, Nanjing 210008, China
[2] Key Laboratory of Particle Astrophysics, Institute of High Energy Physics, Chinese Academy of Sciences, Beijing 100049, China
[3] School of Astronomy and Space Science, University of Science and Technology of China, Hefei 230026, China

Abstract: More than fifty years after the discovery of the knee in the cosmic ray (CR) spectra, its physical origin remains a mystery. This is partly due to the ambiguity of the energy spectra of individual components. Recently, direct measurements from several space experiments found significant spectral hardenings of CR nuclei at ∼200 GV. A joint modeling of the direct and indirect measurements may help to understand the experimental systematics and the physics of the knee. In this work, we update the phenomenological "poly-gonato" model to include the spectral hardenings, with a changing spectral index of $\gamma+\beta\cdot\log E$. This modification gives a reasonable description of the CR spectra in a wide energy range. However, the fits to different data sets give different results. We find that the fit to the AMS-02 and CREAM data slightly favors a relatively low energy knee of the light components. In such a case, the expected all-particle spectra under-shoot the data, which may require an extra component of CRs. The fits to AMS-02 data and the light component (H+He) data from the Tibet ASγ/ARGO-YBJ/WFCTA and KASCADE experiments give consistent results with the all-particle spectra. We further propose a possible physical realization of such a "modified poly-gonato" model of spectral hardenings by means of spatially-dependent diffusion of CRs. We find reasonably good agreement between the model predictions and the data for CR spectra, the secondary-to-primary ratios, and the amplitude of anisotropies.

Keywords: cosmic ray, knee, spectrum, propagation

PACS: 03.30.+p, 02.40.-k **DOI:** 10.1088/1674-1137/42/7/075103

1 Introduction

Nearly sixty years after the discovery of the knee in the cosmic ray (CR) spectra [1], its underlying physical mechanism is still under debate [2]. It is generally accepted that each component has its own knee and the superposition of all components gives the observed break of the all-particle spectra at ~ 4 PeV. This is the so-called "poly-gonato" model [3]. The energy of the knee of each component may be proportional to charge (Z-dependent) or atomic number (A-dependent), which can be used to probe the physical mechanism of the knee [2]. For example, the acceleration limit or propagation leakage may predict a Z-dependence of the knee of each component [4–8]. On the other hand, an A-dependence may imply an interaction origin of the knee, such as photo-disintegration [9, 10], or inelastic collisions between CRs and background photons or neutrinos [11–14].

The energy spectra of individual nuclei components are crucial to understand the knee puzzle. Much effort has been made to measure the individual spectra with air shower experiments. However, no consensus has been achieved yet, primarily due to the systematic uncertainties in the absolute energy calibration. Some progress in the spectral measurements of individual components at PeV energies has been made in recent years with ground-based experiments. Although these measurements themselves are not completely consistent with each other, together they may suggest a knee below PeV for the light components [15–20]. Compared with the ∼4 PeV knee of the all-particle spectra, such a result indicates that the knee is dominated by nuclei heavier than helium [21–23].

The direct measurements of lower energy CRs by balloon-borne or space-based detectors can determine the individual spectra much better. These have been extrapolated to high energies to bridge the direct and air shower experiments [3, 21, 22]. The extrapolation is usually based on power-law fits to the low energy

Received 14 March 2018, Published online 6 June 2018

∗ Supported by National Key Research and Development Program of China (2016YFA0400200), the National Natural Science Foundation of China (11635011, 11761141001, 11663006, 11722328) and the 100 Talents program of Chinese Academy of Sciences

1) E-mail: yuanq@pmo.ac.cn

data. However, remarkable spectral hardenings at rigidities of a few hundred GV in the spectra of all major nuclei components have been reported by the balloon-borne experiments ATIC-2 [24] and CREAM [25], and confirmed with higher precision by the space-based detectors PAMELA [26] and AMS-02 [27, 28]. Many kinds of models have been proposed to understand the origin of the spectral hardenings, including the superposition of different sources [29–31], the non-linear acceleration of supernova remnant shocks [32, 33], the re-acceleration mechanism when particles propagate in the Galaxy [34], and the spatially-dependent diffusion of CRs [35–41].

Given these new measurements of both the direct and indirect experiments, we re-visit the "poly-gonato" model of CRs in this work. We build an updated phenomenological model of the energy spectrum of each component which matches the newest data. We adopt a log-parabolic spectrum with an asymptotically hardening spectral index of $\gamma+\beta\cdot\log E$ to describe the spectral hardenings. An exponential cutoff is employed to describe the knee of CRs. Through fitting to different data sets with the two key parameters, β and the cutoff energy E_c, we further test the consistency among different measurements. One possible physical scenario for such a phenomenological "modified poly-gonato" model is the spatially-dependent diffusion of CRs [35]. In such a model the propagation volume is divided into two regions, the inner halo and the outer halo. The key point is that the diffusion is slower and has a shallower rigidity dependence in the inner halo than in the outer one, which can result in a break in the spectrum. As an illustration of a physical implementation of this "modified poly-gonato" model, we will also discuss this spatially-dependent diffusion scenario and compare its predictions with the observational data.

2 "Modified poly-gonato" model

2.1 Model description

The "poly-gonato" model to describe the knee is basically based on the extrapolation of low-energy measurements. Up to the knee energies, typically three types of models are employed to fit the all-particle spectrum. The first type is motivated by the diffusive shock acceleration or propagation process. In those models, the cutoff energies of CRs are expected to be proportional to the particle charge Z [4, 6]. The second type is motivated by interaction processes, in which the cutoff or break energies are proportional to the atomic number A [9–12]. The third type of break is constant for all species. It is not well physically motivated, but might be a simple assumption [3]. Recent results show that the break energy of light components is lower than that of the all-particle knee, which disfavors this constant break energy scenario [15, 17–19]. Therefore, only the Z-dependent and A-dependent cases are considered in the following discussion.

To include the spectral hardenings at ∼200 GV, we parameterize the spectrum of each component as

$$\begin{aligned}\frac{\mathrm{d}\Phi^i}{\mathrm{d}E}(E) = \Phi^i_0\times&\left(\frac{E}{E_{\rm br}}\right)^{-\gamma^i_1}\\ &\times\left(\frac{1+E/E_{\rm br}}{2}\right)^{\left[\gamma^i_1-\gamma^i_2+\beta\cdot\log(E/E_{\rm had})\right]}\\ &\times\mathrm{e}^{-E/E^i_c},\end{aligned}\tag{1}$$

where $E_{\rm br}$ is the break energy which describes the low energy (with a rigidity of a few GV) behavior of the spectrum, Φ^i_0 is the absolute flux of the ith element at $E_{\rm br}$, $\gamma^i_1(\gamma^i_2)$ is the spectral index below (above) $E_{\rm br}$, $E_{\rm had}$ is the energy characterizing the spectral hardening, which is fixed to be Z·200 GeV, and $\beta\cdot\log(E/E_{\rm had})$ is an asymptotic hardening term used to describe the spectral hardening.

The proton and helium spectra have been measured up to TeV scale by AMS-02 with very high precision [27, 28]. Their spectral parameters are fitted separately with Eq. (1). For the other major components, such as C, O, Mg, Al, Si, and Fe, the HEAO-3 data [42] are used to determine their spectral parameters. For simplicity, their low energy spectral parameters γ_1 and $R_{\rm br}\equiv E_{\rm br}/Z$ are assumed to be the same. For convenience, the spectral parameters of all species are tabulated in the Appendix A.

To account for the spectra around the knee, we assume a Z- or A-dependent cutoff of each species as

$$E^i_c=\begin{cases}E^p_c\cdot Z, & \text{charge dependent}\\ E^p_c\cdot A, & \text{mass dependent}\end{cases}\tag{2}$$

where E^p_c is the cutoff energy of protons. Parameter E^p_c correlates with β. They will be determined through fitting to the data.

2.2 Fitting results

The direct measurements of proton and helium fluxes by AMS-02 [27, 28] and CREAM I+III [43], as well as the air shower array measurements of the light components (H+He) at high energies [15, 17, 18, 20] are used in the fits. The all-particle spectra are not included in the fits. We require that the calculated all-particle spectra are lower than the 2σ upper bounds of the observations. Due to the uncertainties of the absolute energy calibration and the hadronic interaction models of the ground based CR experiments, the observed break energies of the knee of light components differ from each other.

We first classify the ground-based experiments into two groups, the Tibet group (including ASγ, ARGO-YBJ, and WFCTA) and KASCADE. Together with the

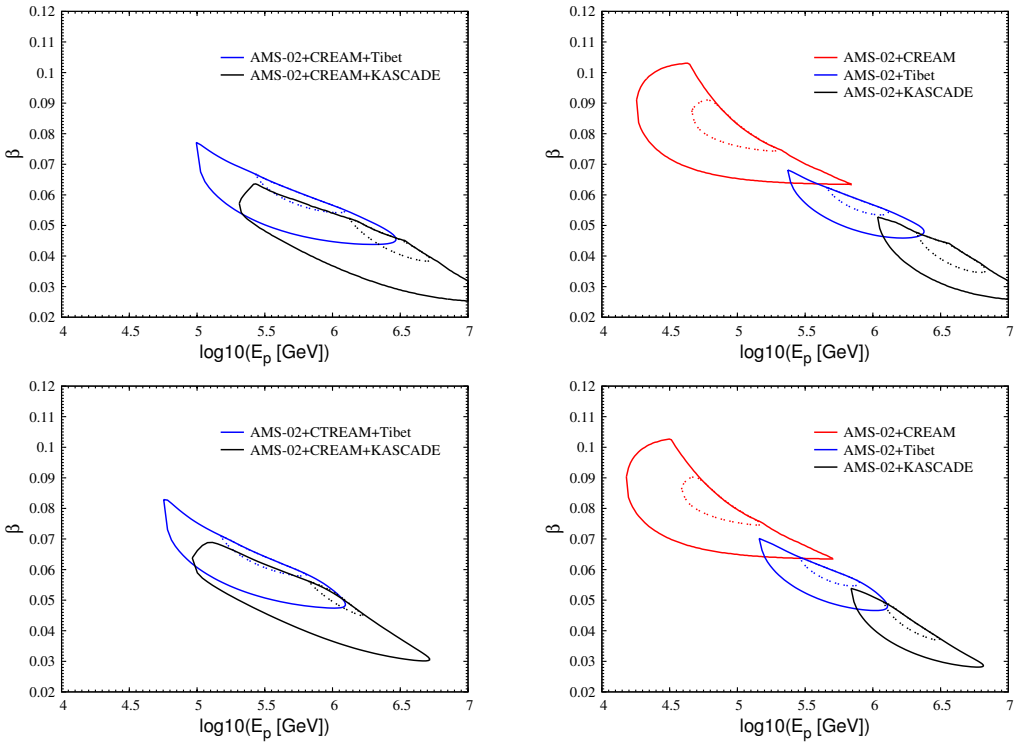

Fig. 1. (color online) The 68% (inner dashed) and 95% (outer solid) confidence regions of parameters β and E_c^p. The left-hand panels are for the combined fits to AMS-02+CREAM+Tibet and AMS-02+CREAM+KASCADE, and the right-hand panels are for the fits to AMS-02+CREAM, AMS-02+Tibet, and AMS-02+KASCADE data, respectively. The upper panels are for Z-dependent and the lower panels are A-dependent cases.

Table 1. Low energy spectral parameters of protons and helium nuclei in the "modified poly-gonato" model.

parameters	Φ_0	$(\mathrm{m^{-2}s^{-1}sr^{-1}GeV^{-1}})$	$R_{\rm br}$	/GV	γ_1		γ_2	
species	p	He	p	He	p	He	p	He
AMS-02+CREAM+Tibet	337.6	9.5	2.15	3.36	−0.63	0.07	2.93	2.84
AMS-02+CREAM+KASCADE	383.0	10.9	1.94	2.94	−0.75	0.00	2.93	2.83
AMS-02+CREAM	290.6	8.0	2.41	4.11	−0.49	0.15	2.96	2.86
AMS-02+Tibet	351.3	9.0	2.07	3.82	−0.69	0.12	2.93	2.84
AMS-02+KASCADE	371.4	10.7	1.99	3.41	−0.70	0.02	2.92	2.82

AMS-02 and CREAM data, we fit to each group of data using both the Z- and A-dependent parameterizations of the knee. The best-fit parameters are given in Tables 1 and 2. The results show that the fit to AMS-02+CREAM+KASCADE data gives a relatively large χ^2 value, while the fit to AMS-02+CREAM+Tibet data is acceptable. This is due to the KASCADE data favoring a relatively high energy of the knee, which requires β to be relatively small, and the spectral hardening effect is not enough to match the CREAM data (see Fig. 1 for the contours of parameters $\log(E_p)$ and β[1)]. To compare with the standard poly-gonato model, we perform the fittings with β=0. The minimum χ^2 values of these fittings are given in Table 2. It is obvious that these fittings are much worse than the "modified poly-gonato" model.

Motivated by the CREAM data possibly revealing a hint of spectral softening above $\sim$ 20 TeV [43], and by the combined fit of AMS-02+CREAM+KASCADE not giving a good enough fit, we separate the CREAM data from the ground-based measurements and re-do the fits with AMS-02+CREAM, AMS-02+Tibet, and AMS-02+KASCADE data, respectively. The favored confidence regions of parameters $\log(E_p)$ and β are shown in the right-hand panels of Fig. 1. It is shown that the AMS-02+CREAM fit tends to favor a relatively low break energy of E_p compared with the other two fits. The parameter regions of AMS-02+Tibet and AMS-

1) An anti-correlation between $\log(E_p)$ and β is shown, which is basically due to a mathematical constraint. For a larger β, the spectra of individual components cannot extend to very high energies without exceeding the all-particle spectra, and hence $\log(E_p)$ is required to be smaller.

Table 2. High energy spectral parameters of the "modified poly-gonato" model.

parameters	mode	AMS-02+CREAM+Tibet	AMS-02+CREAM+KASCADE	AMS-02+CREAM	AMS-02+Tibet	AMS-02+KASCADE
β	Z	0.063	0.045	0.083	0.062	0.041
	A	0.068	0.051	0.083	0.065	0.048
E_c^p	Z	5.7×10^5	2.9×10^6	1.4×10^5	7.4×10^5	3.7×10^6
/GeV	A	2.9×10^5	1.3×10^6	1.3×10^5	4.1×10^5	1.7×10^6
χ^2/dof	Z	128.5/195	225.0/171	68.7/154	63.4/171	76.4/147
χ^2/dof	A	116.7/195	191.1/171	68.5/154	71.7/171	71.6/147
β=0						
χ^2/dof	Z	951.2/196	1042.8/172	678.4/155	653.2/172	399.9/148
χ^2/dof	A	949.4/196	1001.6/172	678.2/155	651.7/172	399.8/148

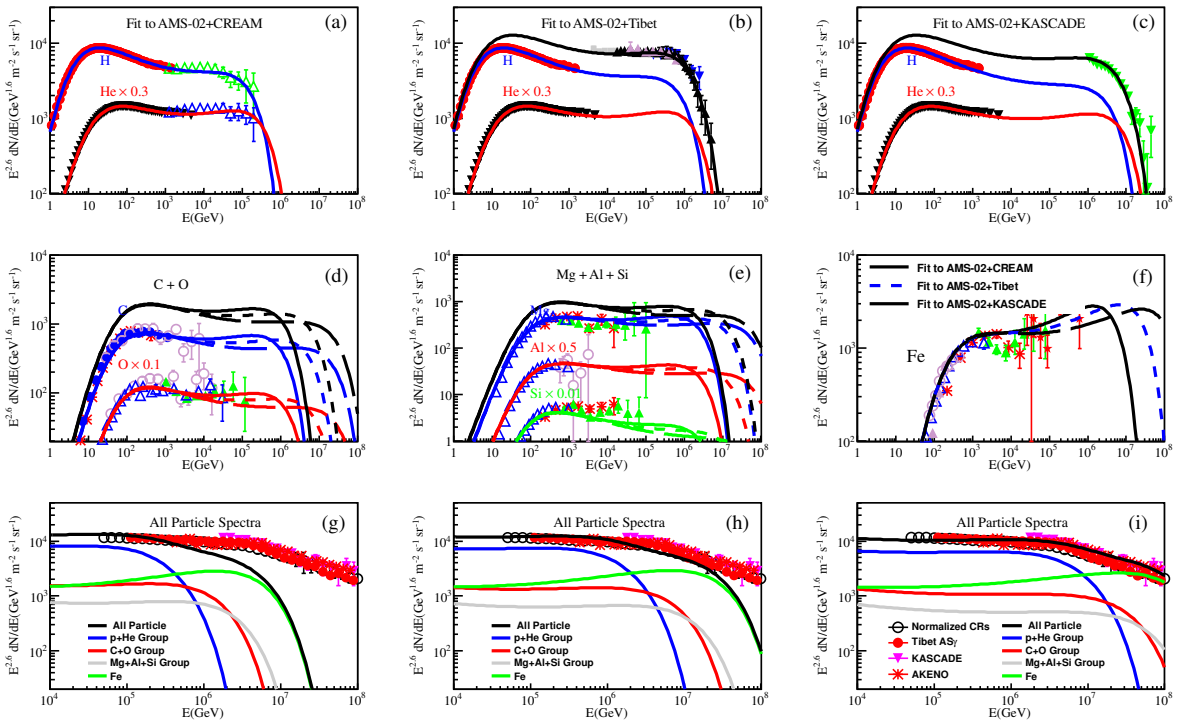

Fig. 2. (color online) The comparison between the best-fit results and the experimental data, for the Z-dependent case. The proton data are from: AMS-02 [27], CREAM [43], and ATIC-2 [24]; the helium data are from: AMS-02 [28], CREAM [43], and ATIC-2 [24]; the carbon, oxygen, magnesium, aluminium, silicon, and iron data are from: HEAO-3 [42], TRACER [44], ATIC-2 [45] and CREAM-II [46]; the proton + helium data are from: KASCADE [16], Tibet-ASγ [15], WFCTA [18], and ARGO-YBJ [17, 19]; and the all-particle data are from: Tibet-ASγ [47], KASCADE [16], Akeno [48], and the normalized average [3].

02+CREAM (AMS-02+KASCADE) overlap with each other at the 95% confidence level. However, the results of AMS-02+CREAM and AMS-02+KASCADE do not overlap.

Figure 2 shows the best-fit results of fluxes of several major components in CRs for the Z-dependent scenario, compared with the data. In this figure, panels (a)-(c) are the spectra of protons, helium, and H+He for the three groups of fits (AMS-02+CREAM, AMS-02+Tibet, and AMS-02+KASCADE). Panel (d) is for C and O, panel (e) is for Mg, Al, and Si, and panel (f) is for Fe. Panels (g)-(i) are the all-particle spectra of the three groups.

We find that for the AMS-02+CREAM fit, the favored energy of the knee of light components is relatively low, which under-shoots the all-particle spectra. However, given the large uncertainties and limited coverage of the energy range of the CREAM data, the constraint on the cutoff energy is very loose (see Fig. 1). The Tibet experimental data gives a median knee energy of light components and is consistent with the all-particle spectra below tens of PeV. The KASCADE data gives the highest energy of the knee, which slightly over-shoots, but is roughly consistent with, the all-particle spectra.

The results for the A-dependent scenario are shown

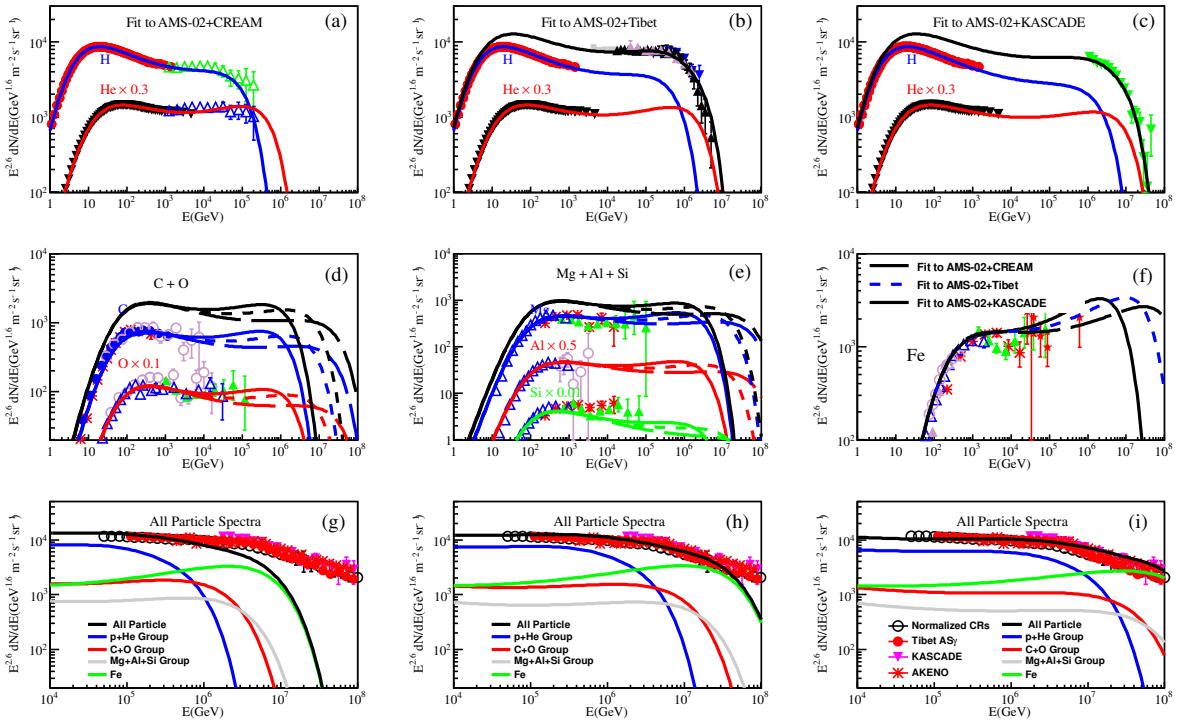

Fig. 3. (color online) The comparison between the best-fit results and the experimental data, for the A-dependent case. The proton data are from: AMS-02 [27], CREAM [43], and ATIC-2 [24]; the helium data are from: AMS-02 [28], CREAM [43], and ATIC-2 [24]; the carbon, oxygen, magnesium, aluminium, silicon, and iron data are from: HEAO-3 [42], TRACER [44], ATIC-2 [45] and CREAM-II [46]; the proton + helium data are from: KASCADE [16], Tibet-ASγ [15], WFCTA [18], and ARGO-YBJ [17, 19]; and the all-particle data are from: Tibet-ASγ [47], KASCADE [16], Akeno [48], and the normalized average [3].

in Fig. 3. We have a similar conclusion to that of the Z-dependent scenario. For the A-dependent case, the knee energy of protons is smaller by a factor of $\sim$2 compared with that of the Z-dependent case. At present it is difficult to distinguish these two cases, and we need measurements of the knee of either protons or helium to distinguish them.

3 Spatially-dependent diffusion model

In the above section, we introduce a "modified poly-gonato" model to reproduce the wide-band spectra of CRs. One possible physical explanation of the spectral hardening ($\beta\cdot\log E$) is the spatially-dependent diffusion of particles [35, 38, 40, 41, 49]. In a simplified version, i.e., CRs diffuse separately in the disk region and halo region (the two-halo model), the hardening of the primary CR nuclei and the excesses of secondary particles can be reasonably accounted for [35, 40, 41, 49]. Here we extrapolate this model to the knee region to reproduce the results of the phenomenological "modified poly-gonato" model.

3.1 Model description

We employ the diffusion reacceleration model to describe the propagation of CR particles [see e.g., 50, 51]. A cylindrical geometry is assumed. The propagation is confined in a halo with half height of z_h. The diffusion coefficient, D_{xx}, depends on both the spatial coordinates (r,z) and the particle rigidity, which is parameterized as [40]

$$D_{xx}(r,z,\rho)=\begin{cases}\eta(r,z)\beta\left(\dfrac{\rho}{\rho_0}\right)^{\varepsilon(r,z)}, & |z|<\xi z_h \ \text{(disk)}\\ D_0\beta\left(\dfrac{\rho}{\rho_0}\right)^{\delta_0}, & |z|>\xi z_h \ \text{(halo)}\end{cases} \quad (3)$$

where β is the velocity of the particle in units of speed of light c, D_0 represents the normalization of the halo diffusion efficient at ρ_0=4 GV, δ_0 characterizes the rigidity dependence of the diffusion coefficient, ξz_h denotes the thickness of the disk, and $\eta(r,z)$ and $\varepsilon(r,z)$ describe the spatial dependence of the diffusion coefficient in the disk. $\eta(r,z)$ and $\varepsilon(r,z)$ can be related to the source distribution $f(r)$, via a unified form, as [40],

$$F(r,z)=\begin{cases}\left(1/[1+e^{f(r)}]-A_i\right)[1-(z/\xi z_h)^4] & \\ \quad +F_0\cdot(z/\xi z_h)^4 & \text{(disk)}\\ F_0 & \text{(halo)}\end{cases} \quad (4)$$

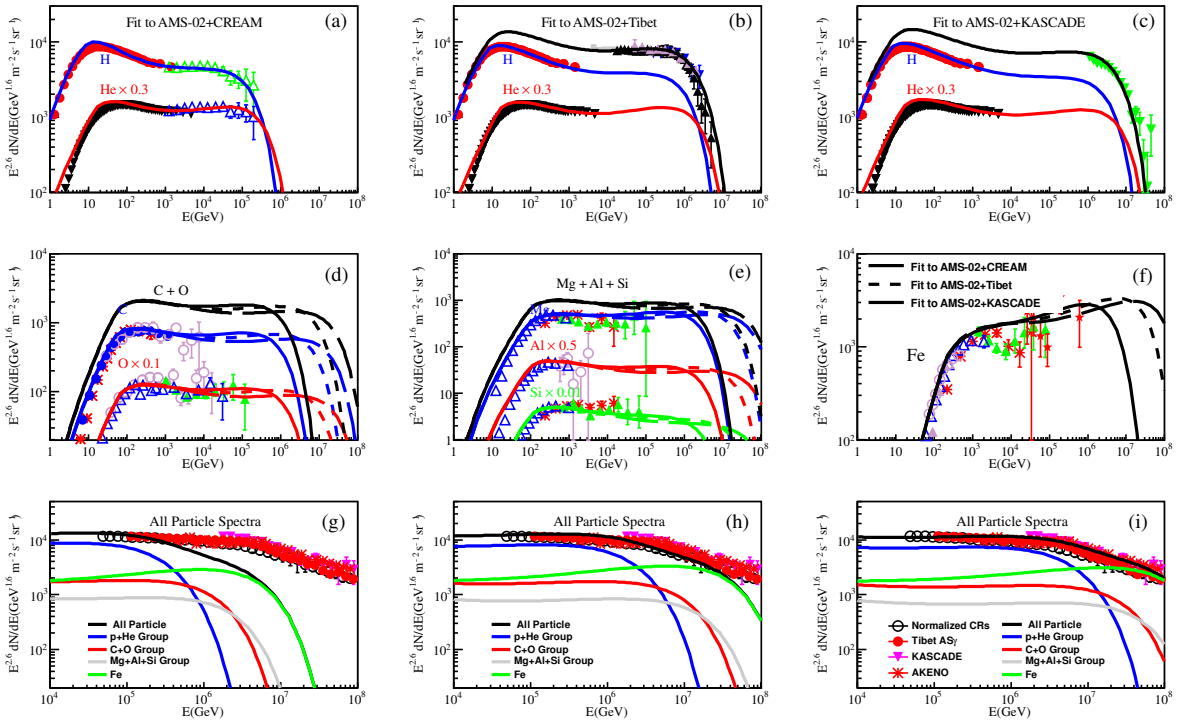

Fig. 4. (color online) The comparison between the best-fit results and the experimental data, for the spatially-dependent diffusion model, for the Z-dependent case. The proton data are from: AMS-02 [27], CREAM [43], and ATIC-2 [24]; the helium data are from: AMS-02 [28], CREAM [43], and ATIC-2 [24]; the carbon, oxygen, magnesium, aluminium, silicon, and iron data are from: HEAO-3 [42], TRACER [44], ATIC-2 [45] and CREAM-II [46]; the proton + helium data are from: KASCADE [16], Tibet-ASγ [15], WFCTA [18], and ARGO-YBJ [17, 19]; and the all-particle data are from: Tibet-ASγ [47], KASCADE [16], Akeno [48], and the normalized average [3].

where A_i is a constant with i denoting η or ε, and F_0 is the D_0 and δ_0.

The reacceleration is described by a diffusion in momentum space, with a relation between $D_{\rm pp}$ and $D_{\rm xx}$ of [52]

$$D_{pp}D_{xx}=\frac{4p^2v_A^2}{3\delta(4-\delta^2)(4-\delta)w}, \tag{5}$$

where p is the momentum of a particle, δ is the power-law index of the rigidity dependence of the spatial diffusion coefficient (see Eq. (3)), v_A is the Alfven speed, and w is the ratio of the magnetohydrodynamic wave energy density to the magnetic field energy density, which is assumed to be 1.

The injection spectrum of CR nuclei is assumed to be a broken power-law with an exponential cutoff

$$q_{\rm inj}(E)=q_0{\rm e}^{-E/E_c^i}\times\begin{cases}(E/E_{\rm br})^{-\gamma_1}, & E<E_{\rm br}\\ (E/E_{\rm br})^{-\gamma_2}, & E\geqslant E_{\rm br}\end{cases}. \tag{6}$$

where q_0 is the normalization factor, $E_{\rm br}$ is the break energy, γ_1,γ_2 are the spectral indices below and above $E_{\rm br}$, and E_c^i characterizes the spectral cutoff around the knee. The relative abundances of different nuclei are adopted as the default values used in DRAGON [53]. Similar to Section 2, we consider both Z-dependent and A-dependent models for the cutoff.

Low energy particles ($E\lesssim$10 GeV/n) will be modulated by solar activity, showing suppression of their low energy fluxes. We use the force-field approximation to account for this solar modulation [54]. In this work, the modulation potential Φ is fixed to be 550 MV for all the nuclei except for B/C, whose modulation potential is adopted as 200 MV.

3.2 Results

3.2.1 Primaries

We use the numerical code DRAGON to calculate the spatial dependent diffusion of CRs [53]. The injection spectral parameters are given in Tables 3. The parameter γ_2 differs for each species. They are tuned to fit the data for the major components. For the less abundant nuclei, we assume the same difference of γ_2 from that of protons, as in Section 2. The full compilation of γ_2 is given in the Appendix A.

The propagation parameters are given in Table 4. Note that, in principle, the allowed parameter space needs to be estimated by a global fit to the data, which is CPU-time consuming and is left for future studies.

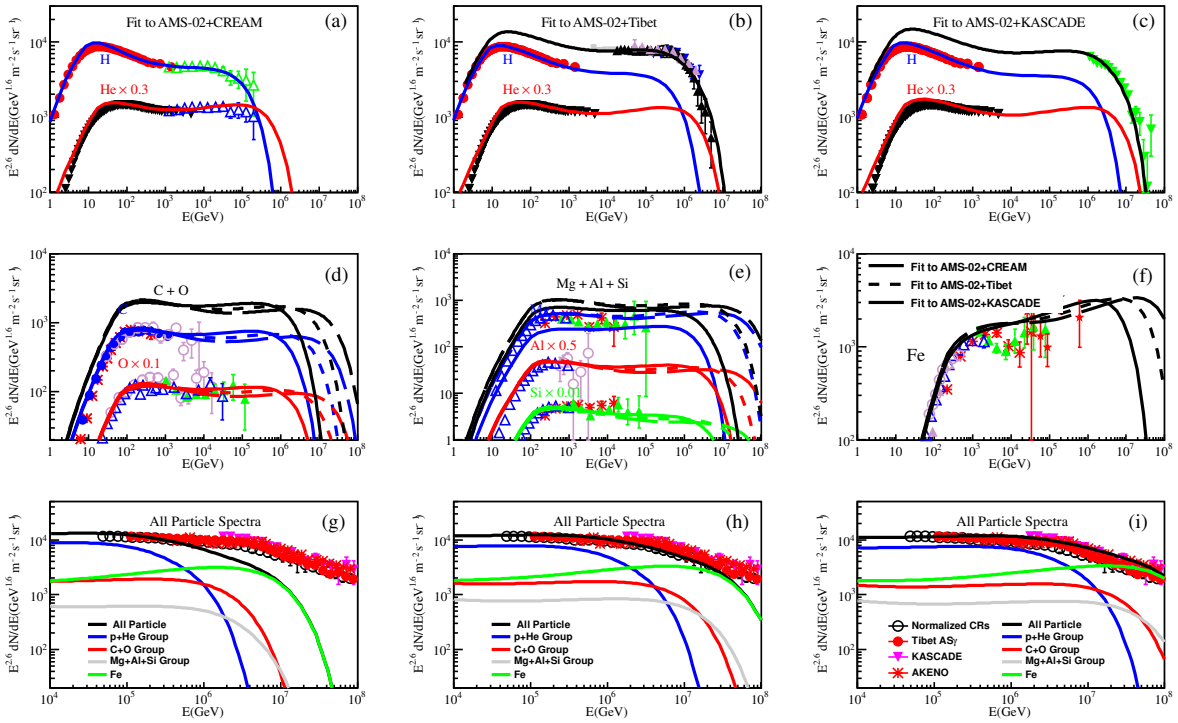

Fig. 5. (color online) The comparison between the best-fit results and the experimental data, for the spatially-dependent diffusion model, for the A-dependent case. The proton data are from: AMS-02 [27], CREAM [43], and ATIC-2 [24]; the helium data are from: AMS-02 [28], CREAM [43], and ATIC-2 [24]; the carbon, oxygen, magnesium, aluminium, silicon, and iron data are from: HEAO-3 [42], TRACER [44], ATIC-2 [45] and CREAM-II [46]; the proton + helium data are from: KASCADE [16], Tibet-ASγ [15], WFCTA [18], and ARGO-YBJ [17, 19]; and the all-particle data are from: Tibet-ASγ [47], KASCADE [16], Akeno [48], and the normalized average [3].

Table 3. Injection parameters of the "spatially-dependent diffusion" model.

	E_{br}/GV	γ_1	E_c^p/GeV	
mode			Z	A
AMS-02+CREAM	9.5	1.85	1.8×10^5	1.5×10^5
AMS-02+Tibet	9.5	1.85	1.1×10^6	6.6×10^5
AMS-02+KASCADE	9.5	1.85	3.9×10^6	2.0×10^6

Table 4. Propagation parameters of the "spatially-dependent diffusion" model.

	AMS-02+CREAM	AMS-02+Tibet	AMS-02+KASCADE
$D_0/(\mathrm{cm}^2/\mathrm{s})$	6.8×10^{28}	6.8×10^{28}	6.8×10^{28}
δ_0	0.58	0.52	0.5
$v_A/(\mathrm{km/s})$	16	16	16
z_h/kpc	5	5	5
ξ	0.14	0.12	0.11
A_η	0.10	0.10	0.10
A_ε	−0.17	−0.16	−0.14

We compare the model predictions to the three data sets of the knee of the light components, as described in Section 2. Results for the primary CRs are shown in Figs. 4 and 5, for the Z- and A-dependent cutoff scenarios of the knee respectively. We find that the results are very similar to that of the "modified poly-gonato" model. It is shown that a log-parabolic shape of the energy spectrum is a good approximation of a class of models with smooth hardenings.

3.2.2 Secondaries

Secondary particles are produced by collisions of primary CRs with the interstellar medium when they propagate in the Galaxy. It is believed that most antiprotons and boron nuclei are such secondaries, which can be very effective to probe the particle propagation process. We calculate the expected $\bar{p}/p$ and B/C ratios of this spatially-dependent diffusion model, as shown in Fig. 6. These results are reasonably consistent with the observational data. However, we do find that the secondary-to-primary ratio becomes asymptotically flatter at high energies, which is different from the simple uniform diffusion scenario. This can be tested with future observations of the B/C ratio at higher energies.

3.2.3 Anisotropy

The flow of CRs will form a dipole anisotropy of arrival directions when observed at a fixed point. We calculate the amplitude of the dipole anisotropy of CRs as

$$A=\frac{3D}{c}\frac{\nabla\phi}{\phi}, \tag{7}$$

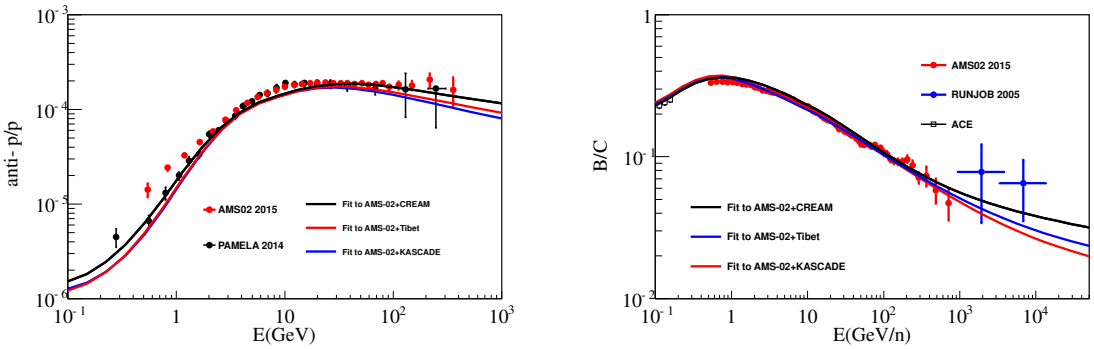

Fig. 6. (color online) The calculated $\bar{p}/p$ (left panel) and B/C (right panel) ratios of the spatially-dependent diffusion model. The $\bar{p}/p$ data are from AMS-02 [55] and PAMELA [56]; the B/C data are from AMS-02 [55], ACE [57] and RUNJOB [58].

where ϕ is the locally observed differential fluxes of CRs. The dipole anisotropy amplitude as a function of energy is given in Fig. 7. The amplitude of the anisotropy is smaller than the prediction of the standard diffusion model [35, 40, 41, 49], and is consistent with observations up to a few tens of TeV. Note, however, the phase of the observed anisotropy shows an evolution with energy, which cannot be simply accounted for by the diffusion process [59]. More complicated processes like the effect of the local magnetic field and/or local sources may be responsible for it [60].

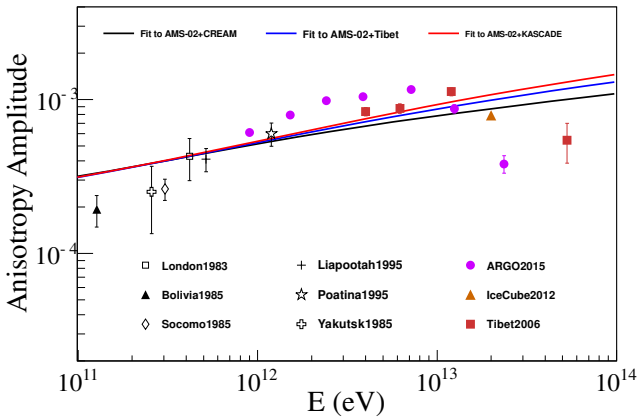

Fig. 7. (color online) The calculated anisotropy of CRs for the spatially-dependent diffusion model. The data are from underground muon observations: London1983 [61], Bolivia1985 [62], Socorro1985 [62], Yakutsk1985 [62], Liapootah1995 [63], and Poatina1995 [64], and air shower array experiments: Tibet2006 [65], IceCube2012 [66], and ARGO2015 [67].

4 Discussion and conclusions

Recent observations have revealed new features in the CR spectra, including spectral hardenings at $\sim$200 GV rigidities from balloon or space detectors and the knee of light components (p and He) from air shower experiments. In this work we develop a modified version of the "poly-gonato" model of the knee, taking into account such new data. A log-parabolic term of the spectrum is employed to describe the spectral hardenings. As for the knee, we adopt an exponential cutoff spectrum to describe it, with the cutoff energy being proportional to Z or A of each species. We then fit the spectral parameters to the observational data. Due to the difficulty of absolute energy calibration in the air shower experiments, the break positions of the light component spectra differ to some degree among different experiments. Therefore the fits are done for different datasets separately, based on the light component measurements by CREAM, the Tibet experiments (ASγ, WFCTA and ARGO-YBJ), and KASCADE. We also try to jointly fit the CREAM data and the air shower experimental data, and find that the fitting goodness is relatively poor, expecially for CREAM+KASCADE. In all the fits, the AMS-02 measurements at low energies ($\lesssim$TeV) are included.

The results show that the knee energies inferred from different data groups are marginally consistent with each other. The CREAM data slightly favors a relatively low energy knee of protons and helium nuclei, which undershoots the all-particle spectra individual fits. In this case, an extra component of CRs below the knee may be required [e.g., 23, 68]. The Tibet experiment and KASCADE data of light components are roughly consistent with the all-particle data.

There are no good measurements of CR spectra in the energy range of 1$-$100 TeV. For example, the proton and helium spectra measured by CREAM [43] differ greatly from those measured by ATIC-2 [24]. A direct comparison of the AMS-02 and CREAM helium fluxes shows that the CREAM fluxes are higher by about 20% at TeV/nucleon [28]. Further more precise measurements of the energy spectra of various species, by e.g., CALET [69], DAMPE [70], and LHAASO [71] will be very im-

portant to better determine the model parameters.

It is also possible that the fitting function, which is basically smooth at the hardening and cutoff, is not good enough to describe the data. If there are some sharp structures in the spectra, the CREAM proton and helium spectra and the all-particle data might be more consistent with each other. However, in such a case the model may need fine tuning.

Finally, we give a physical model with spatially-dependent diffusion of CRs to reproduce the results of this phenomenological "modified poly-gonato" model. Apart from the potential inconsistencies among different data sets, the energy spectra of the primary CRs, the secondary-to-primary ratios, and the amplitude of the anisotropy are shown to be consistent with observations. This model predicts asymptotic hardening of the B/C ratio above hundreds of TeV/n, which can also be tested with future measurements.

Appendix A

We present the spectral parameters of all nuclei up to iron as used in this work.

Table A1. Low energy spectral parameters of all nuclei of the "modified poly-gonato" model (Section 2).

Z	$E_{\rm br}/Z$ /GV	Φ_0 /($\rm m^{-2}s^{-1}sr^{-1}GeV^{-1}$)	γ_1	γ_2
3	5.38	8.87×10^{-3}	0.25	2.73
4	5.38	5.57×10^{-3}	0.25	2.94
5	5.38	1.56×10^{-2}	0.25	3.44
6	5.38	4.44×10^{-2}	0.25	2.85
7	5.38	7.75×10^{-3}	0.25	2.91
8	5.38	3.12×10^{-2}	0.25	2.87
9	5.38	5.08×10^{-4}	0.25	2.88
10	5.38	3.52×10^{-3}	0.25	2.83
11	5.38	7.09×10^{-4}	0.25	2.85
12	5.38	4.50×10^{-3}	0.25	2.83
13	5.38	8.00×10^{-4}	0.25	2.85
14	5.38	3.50×10^{-3}	0.25	2.94
15	5.38	1.02×10^{-4}	0.25	2.88
16	5.38	4.36×10^{-4}	0.25	2.74
17	5.38	8.81×10^{-5}	0.25	2.87
18	5.38	1.36×10^{-4}	0.25	2.83
19	5.38	1.02×10^{-4}	0.25	2.84
20	5.38	2.30×10^{-4}	0.25	2.89
21	5.38	4.20×10^{-5}	0.25	2.83
22	5.38	1.26×10^{-4}	0.25	2.80
23	5.38	7.00×10^{-5}	0.25	2.82
24	5.38	1.10×10^{-4}	0.25	2.86
25	5.38	1.00×10^{-4}	0.25	2.71
26	5.38	1.05×10^{-3}	0.25	2.73

Table A2. Injection spectral parameters γ_2 of all nuclei of the "spatially-dependent diffusion" model (Section 3).

symbol	Z	γ_2
H	1	2.43
He	2	2.36
Li	3	2.26
Be	4	2.47
B	5	2.67
C	6	2.38
N	7	2.44
O	8	2.40
F	9	2.41
Ne	10	2.36
Na	11	2.38
Mg	12	2.36
Al	13	2.38
Si	14	2.47
P	15	2.41
S	16	2.27
Cl	17	2.40
Ar	18	2.36
K	19	2.37
Ca	20	2.42
Sc	21	2.36
Ti	22	2.33
V	23	2.35
Cr	24	2.39
Mu	25	2.18
Fe	26	2.31

References

1 G. V. Kulikov and G. B. Kristiansen, J. Exp. Theor. Phys., **35**: 635 (1958)
2 J. R. Hörandel, Astroparticle Physics, **21**: 241–265 (2004)
3 J. R. Hörandel, Astroparticle Physics, **19**: 193–220 (2003)
4 P. O. Lagage and C. J. Cesarsky, Astron. Astrophys., **125**: 249–257 (1983)
5 H. J. Voelk and P. L. Biermann, Astrophys. J. Lett., **333**: L65–L68 (1988)
6 V. S. Ptuskin, S. I. Rogovaya, V. N. Zirakashvili et al, Astron. Astrophys., **268**: 726–735 (1993)
7 E. G. Berezhko, Astroparticle Physics, **5**: 367–378 (1996)
8 B. Wiebel-Sooth, P. L. Biermann, and H. Meyer, Astron. Astrophys., **330**: 389–398 (1998)
9 S. Karakula and W. Tkaczyk, Astroparticle Physics, **1**: 229–237 (1993)
10 J. Candia, L. N. Epele, and E. Roulet, Astroparticle Physics, **17**: 23–33 (2002)
11 D. Kazanas and A. Nicolaidis, International Cosmic Ray Conference, **5**: 1760 (2001)
12 H.-B. Hu, Q. Yuan, B. Wang et al, Astrophys. J. Lett., **700**:

L170–L173 (2009)
13 B. Wang, Q. Yuan, C. Fan et al, Science China Physics, Mechanics, and Astronomy, **53**: 842–847 (2010)
14 Y.-Q. Guo, Z.-Y. Feng, Q. Yuan, C. Liu, and H.-B. Hu, New Journal of Physics, **15**(1): 013053 (2013)
15 J. Huang, Primary proton and helium spectra at energy range from 50 TeV to 1PeV observed with (YAC+Tibet-III) hybrid experiment, International Cosmic Ray Conference, 2013
16 W. D. Apel, J. C. Arteaga-Velázquez, K. Bekk et al, Astroparticle Physics, **47**: 54–66 (2013)
17 S. M. Mari, P. Montini, and for the ARGO-YBJ Collaboration, Phys. Rev. D, **91**: 112017 (2015)
18 B. Bartoli, P. Bernardini, X. J. Bi et al, Phys. Rev. D, **92**(9): 092005 (2015)
19 A. D'Amone, I. De Mitri, and A. Surdo, Measurement of the cosmic ray all-particle and light-component energy spectra with the ARGO-YBJ experiment, arXiv:1502.04840
20 P. Montini and S. M. Mari, The bending of the proton plus helium flux in primary cosmic rays measured by the ARGO-YBJ experiment in the energy range from 20 TeV to 5 PeV, arXiv:1608.01389
21 M. Shibata, Y. Katayose, J. Huang, and D. Chen, Astrophys. J., **716**: 1076–1083 (2010)
22 Y. Zhao, H.-Y. Jia, and F.-R. Zhu, Chinese Physics C, **39**(12): 125001 (2015)
23 S. Thoudam, J. P. Rachen, A. van Vliet et al, Astron. Astrophys., **595**: A33 (2016)
24 A. D. Panov, J. H. Adams, Jr., H. S. Ahn et al, Bulletin of the Russian Academy of Science, Phys., **71**: 494–497 (2007)
25 H. S. Ahn, P. Allison, M. G. Bagliesi et al, Astrophys. J. Lett., **714**: L89–L93 (2010)
26 O. Adriani, G. C. Barbarino, G. A. Bazilevskaya et al, Science, **332**: 69 (2011)
27 M. Aguilar, D. Aisa, B. Alpat et al, Physical Review Letters, **114**(17): 171103 (2015)
28 M. Aguilar, D. Aisa, B. Alpat et al, Physical Review Letters, **115**(21): 211101 (2015)
29 V. I. Zatsepin and N. V. Sokolskaya, Astron. Astrophys., **458**: 1–5 (2006)
30 Q. Yuan, B. Zhang, and X.-J. Bi, Phys. Rev. D, **84**(4): 043002 (2011)
31 S. Thoudam and J. R. Hörandel, Mon. Not. Roy. Astron. Soc., **421**: 1209–1214 (2012)
32 P. L. Biermann, J. K. Becker, J. Dreyer et al, Astrophys. J., **725**: 184–187 (2010)
33 V. Ptuskin, V. Zirakashvili, and E.-S. Seo, Astrophys. J., **763**: 47 (2013)
34 S. Thoudam and J. R. Hörandel, Astron. Astrophys., **567**: A33 (2014)
35 N. Tomassetti, Astrophys. J. Lett., **752**: L13 (2012)
36 D. Gaggero, D. Grasso, A. Marinelli, A. Urbano, and M. Valli, Astrophys. J. Lett., **815**: L25 (2015)
37 N. Tomassetti, Phys. Rev. D, **92**(8): 081301 (2015)
38 C. Jin, Y.-Q. Guo, and H.-B. Hu, Chinese Physics C, **40**(1): 015101 (2016)
39 Y. Q. Guo, H. B. Hu, and Z. Tian, Chinese Physics C, **40**: 115001 (2016)
40 Y.-Q. Guo, Z. Tian, and C. Jin, Astrophys. J., **819**: 54 (2016)
41 J. Feng, N. Tomassetti, and A. Oliva, Phys. Rev. D, **94**(12): 123007 (2016)
42 J. J. Engelmann, P. Ferrando, A. Soutoul, P. Goret, and E. Juliusson, Astron. Astrophys., **233**: 96–111 (1990)
43 Y. S. Yoon, T. Anderson, A. Barrau et al, Astrophys. J., **839**: 5 (2017)
44 M. Ave, P. J. Boyle, F. Gahbauer et al, Astrophys. J., **678**: 262–273 (2008)
45 A. D. Panov, J. H. Adams, H. S. Ahn et al, Bulletin of the Russian Academy of Sciences, Physics, **73**: 564–567 (2009)
46 H. S. Ahn, P. Allison, M. G. Bagliesi et al, Astrophys. J., **707**: 593–603 (2009)
47 M. Amenomori, X. J. Bi, D. Chen et al, Astrophys. J., **678**: 1165–1179 (2008)
48 M. Nagano, T. Hara, Y. Hatano et al, Journal of Physics G Nuclear Physics, **10**: 1295–1310 (1984)
49 N. Tomassetti, Phys. Rev. D, **92**(6): 063001 (2015)
50 A. W. Strong, I. V. Moskalenko, and V. S. Ptuskin, Annual Review of Nuclear and Particle Science, **57**: 285–327 (2007)
51 Q. Yuan, S.-J. Lin, K. Fang, and X.-J. Bi, Phys. Rev. D, **95**(8): 083007 (2017)
52 E. S. Seo and V. S. Ptuskin, Astrophys. J., **431**: 705–714 (1994)
53 C. Evoli, D. Gaggero, D. Grasso, and L. Maccione, Journal of Cosmology and Astroparticle Physics, **10**: 18 (2008)
54 L. J. Gleeson and W. I. Axford, Astrophys. J., **154**: 1011 (1968)
55 AMS-02 collaboration, Talks at the 'AMS Days at CERN', 15-17 April, 2015
56 O. Adriani, G. C. Barbarino, G. A. Bazilevskaya et al, Physics Reports, **544**: 323 (2014)
57 A. J. Davis, R. A. Mewaldt, W. R. Binns et al, On the low energy decrease in galactic cosmic ray secondary/primary ratios, In R. A. Mewaldt, J. R. Jokipii, M. A. Lee, E. Möbius, and T. H. Zurbuchen, editors, Acceleration and Transport of Energetic Particles Observed in the Heliosphere, volume 528 of American Institute of Physics Conference Series, pages 421–424, September 2000
58 V. A. Derbina, V. I. Galkin, M. Hareyama et al, Astrophys. J. Lett., **628**: L41–L44 (2005)
59 M. Amenomori and et al, International Cosmic Ray Conference, 2015
60 M. Ahlers, Deciphering the Dipole Anisotropy of Galactic Cosmic Rays, Physical Review Letters, **117**: 151103 (2016)
61 T. Thambyahpillai, International Cosmic Ray Conference, **3**: 383 (1983)
62 D. B. Swinson and K. Nagashima, Planet. Space Sci., **33**: 1069–1072 (1985)
63 K. Munakata, S. Yasue, S. Mori et al, International Cosmic Ray Conference, **4**: 639 (1995)
64 K. B. Fenton, A. G. Fenton, and J. E. Humble, International Cosmic Ray Conference, **4**: 635 (1995)
65 M. Amenomori, S. Ayabe, X. J. Bi et al, Science, **314**: 439–443 (2006)
66 R. Abbasi, Y. Abdou, T. Abu-Zayyad et al, Astrophys. J., **746**: 33 (2012)
67 B. Bartoli, P. Bernardini, X. J. Bi et al, Astrophys. J., **809**: 90 (2015)
68 T. K. Gaisser, T. Stanev, and S. Tilav, Frontiers of Physics, **8**: 748–758 (2013)
69 CALET Collaboration, Nuclear Physics B Proceedings Supplements, **166**: 43–49 (2007)
70 J. Chang et al, Astropart. Phys., **95**: 6 (2017)
71 Z. Cao, Chinese Physics C, **34**: 249–252 (2010)